Imaging Spin Flows in Semiconductors Subject to Electric, Magnetic, and Strain Fields

S. A. Crooker and D. L. Smith

Los Alamos National Laboratory, Los Alamos, New Mexico 87545, USA

(Received 18 November 2004; published 15 June 2005)

Using scanning Kerr microscopy, we directly acquire two-dimensional images of spin-polarized electrons flowing laterally in bulk epilayers of *n*:GaAs. Optical injection provides a local dc source of polarized electrons, whose subsequent drift and/or diffusion is controlled with electric, magnetic, and—in particular—strain fields. Spin precession induced by controlled uniaxial stress along the $\langle 110 \rangle$ axes demonstrates the direct $\mathbf{k}$-linear spin-orbit coupling of electron spin to the shear (off diagonal) components of the strain tensor, ϵ_{xy}.

DOI: 10.1103/PhysRevLett.94.236601 PACS numbers: 72.25.Dc, 71.70.Ej, 85.75.−d

The ability to control and measure electron spin degrees of freedom in semiconductors has been proposed as the operating principle for a new generation of novel ''spintronic'' devices [1,2]. Semiconductor devices utilizing electron spin generally require: (i) transport of spin-polarized electrons from one location in the device to another, and (ii) a means to manipulate the electron spin orientation, either directly with magnetic fields or indirectly with electric and/or strain fields that exploit the spin-orbit interaction. Many of these device proposals [3–6] are based on a field-effect transistor geometry in which electron transport occurs in essentially two-dimensional structures. In order to design semiconductor structures whose function is based on electron spin it is necessary to understand the transport and flow of spin-polarized electrons, and how it is influenced by electric, magnetic, and strain fields in these 2D structures.

Using methods for scanning Kerr microscopy, we acquire 2D images of spin-polarized conduction electrons flowing laterally in bulk epilayers of *n*-type GaAs. The images directly reveal the spatial dependence of spin diffusion and spin drift in the presence of applied electric, magnetic, and—in particular—strain fields. Controlled uniaxial stress along the $\langle 110 \rangle$ axes induces spin precession, revealing the direct ($\mathbf{k}$-linear) spin-orbit coupling of electron spin to the off diagonal components of the strain tensor $\boldsymbol{\epsilon}$. The coupling may be characterized by an effective strain-induced magnetic field $\mathbf{B}_{\boldsymbol{\epsilon}}$, which is shown to be orthogonal to the electron momentum $\mathbf{k}$, and therefore chiral for radially-diffusing spins. $\mathbf{B}_{\boldsymbol{\epsilon}}$ scales linearly with $|\mathbf{k}|$, yielding a spatial precession of electron spins that is independent of electrical bias and is considerably more robust against the randomizing (ensemble dephasing) effects of spin diffusion as compared with precession induced by external magnetic fields.

The samples are 1 μm thick, silicon-doped (*n*-type) GaAs epilayers grown by molecular beam epitaxy on [001]-oriented semi-insulating GaAs substrates. Doping densities are $n_e = 1$, 5, and $10 \times 10^{16}/\mathrm{cm}^3$. Pieces were cleaved along the [110] and $[1\bar{1}0]$ natural cleave directions, and ohmic contacts allowed an in-plane, lateral electrical bias in the [110] direction. The samples were mounted in vacuum on the cold finger of an optical cryostat. To apply controlled uniaxial stress along the [110] or $[1\bar{1}0]$ axis at low temperature, the cold finger incorporated a small cryogenic vise, whose lead screw was adjusted via a retractable actuator. Since all the samples exhibited qualitatively similar strain-related effects, we show data from only the $n_e = 10^{16}/\mathrm{cm}^3$ epilayer.

A local, steady-state source of electrons, spin polarized along the sample normal ([001], or $\hat{z}$), was provided by a circularly-polarized 1.58 eV diode laser focused to a 4 μm spot on the epilayer. While this pump laser (10–25 μW) injects spin-polarized electrons *and* holes, the holes spin relax and recombine rapidly, leaving a net spin polarization of the mobile conduction electrons [7]. These electrons subsequently drift and/or diffuse laterally away from the point of generation. 2D images of the resulting z component of electron spin were acquired by measuring the polarization (Kerr) rotation imparted on a linearly polarized probe laser that was reflected from the epilayer surface and raster scanned in the x-y epilayer plane. The probe beam (50–100 μW) was derived from a tunable cw Ti:sapphire laser, and also focused to a 4 μm spot. For lock-in measurement, the pump laser polarization was modulated from left- to right-circular (injecting spins along $\pm\hat{z}$) at 50 kHz.

The measured Kerr rotation is a strong function of probe photon energy near the GaAs band edge [inset, Fig. 1(a)]. Here, 30 μm separates the pump and probe spots, so that the signal arises solely from a nonzero spin polarization of the electron Fermi sea. This energy-dependent response provides a relative (and *in situ*) monitor of stress-induced band edge shifts. When imaging, the probe energy is tuned (as shown) *below* the 1.515 eV GaAs band edge, to minimize perturbation of the Fermi sea.

Figure 1(a) shows a 70×140 μm image of the steady-state electron spin polarization in the $n_e = 10^{16}/\mathrm{cm}^3$ GaAs epilayer due to spin diffusion alone. To emphasize smaller signals, the color scale has been adjusted so that white equals half the peak signal. The spatial extent of the measured spin polarization (~ 60 μm edge to edge) is

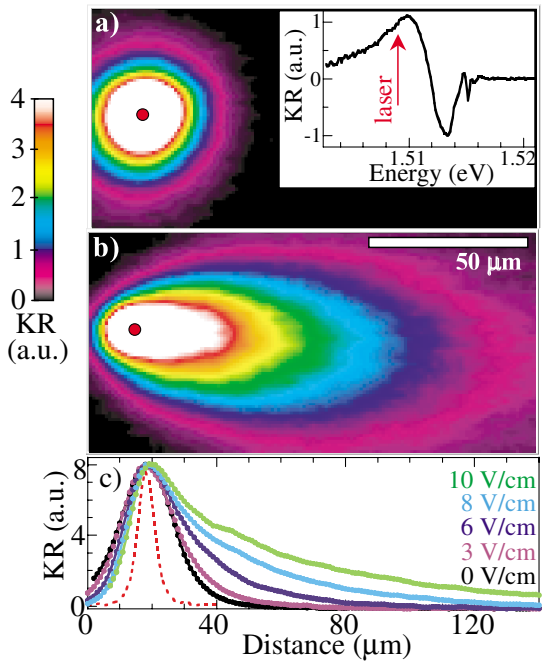

FIG. 1 (color). (a) 70×140 μm image of electron spin polarization in a 1 μm thick n:GaAs epilayer ($n_e = 10^{16}$ cm^{-3}) at 4 K, acquired via Kerr-rotation (KR) microscopy. A circularly polarized 1.58 eV laser focused to a 4 μm spot provides a local, dc source of spin-polarized electrons; this image indicates 2D spin diffusion. Inset: KR vs probe photon energy near the 1.515 eV GaAs band edge. (b) With $E = 10$ V/cm lateral electrical bias, showing spin diffusion and drift. (c) Cross sections of spin flow vs bias; dotted line shows 5.5 μm resolution.

much larger than the focused pump laser (shown by the red spot), indicating diffusion of electron spins away from the point of generation. Images of radially-diffusing electrons provide information on spin flows along *all* $\mathbf{k}$ directions in the x-y sample plane, which will prove useful later in confirming the direction of $\mathbf{B}_\epsilon$. The characteristic diffusion length is given by the electron spin lifetime $\tau_s = 120$ ns (measured independently via ultrafast techniques) and spin diffusion constant D_s. Fits to a 2D drift-diffusion model (described later) indicate $D_s \simeq 3$ and 15 cm^2/s for the $n_e = 1$ and 5×10^{16}/cm^3 samples at 4 K, respectively, values in accord with the charge diffusion constants. Spin-polarized electrons can also be induced to drift laterally along an applied electric field E [Fig. 1(b)]. This "spin drag," as revealed by Kikkawa and Awschalom [7], occurs over lengths >100 μm. 2D images of spin drift and diffusion [Fig. 1(b), where $E = 10$ V/cm] show roughly elliptical contours of constant spin polarization, with the major axis determined by electrical bias and lateral spin flow extending beyond 150 μm. Figure 1(c) shows normalized line cuts through a series of images.

Spin-orbit coupling in GaAs permits coupling to electron spin degrees of freedom through the *spatial* part of the electron wave function, thus allowing induced precession of electron spins *without* external magnetic fields [8–10]. Spin-orbit effects lead to spin splittings of the conduction band along particular crystal momenta $\mathbf{k}$, and can be characterized by effective magnetic fields. Bulk inversion asymmetry arises from the lack of inversion symmetry in GaAs, leading to a spin splitting for electrons with $\mathbf{k}$ along the $\langle 110 \rangle$ axes (but no splitting along $\langle 111 \rangle$ or $\langle 100 \rangle$ axes). This ubiquitous coupling, cubic in $|\mathbf{k}|$, is the origin of the D'yakonov-Perel' mechanism of electron spin relaxation in bulk GaAs. A second spin-orbit effect arises from structural inversion asymmetry (the "Rashba" term [11]), as typically found in 2D heterostructures. Inversion asymmetry of the confining potential along the growth direction $\hat{z}$ (typically [001]) can often be characterized by an electric field $\mathbf{E}_z$, giving a Rashba Hamiltonian $H_R \propto \boldsymbol{\sigma} \cdot (\mathbf{k} \times \mathbf{E}_z)$. For typical 2D heterostructures with $\mathbf{k}$ in the x-y plane, the effective magnetic field $\mathbf{k} \times \mathbf{E}_z$ is therefore in plane and orthogonal to $\mathbf{k}$, with magnitude linear in $|\mathbf{k}|$. Control of the Rashba spin-orbit term, through a gate-tunable $\mathbf{E}_z$, is the basis of the original Datta-Das spin transistor [3].

Figure 2 demonstrates an additional spin-orbit effect; namely, the coupling of the electron spin to the strain tensor $\boldsymbol{\epsilon}$. As described previously [12–15], stress along the $\langle 110 \rangle$ axes of GaAs induces $\mathbf{k}$-linear spin splittings in the conduction band through the off diagonal (shear) elements of $\boldsymbol{\epsilon}$. The strain Hamiltonian is $H_S = c_3 \boldsymbol{\sigma} \cdot \boldsymbol{\varphi}$, where $(\varphi_x, \varphi_y, \varphi_z) = (\epsilon_{xy} k_y - \epsilon_{xz} k_z, \epsilon_{yz} k_z - \epsilon_{yx} k_x, \epsilon_{zx} k_x - \epsilon_{zy} k_y)$, (x, y, z) are the principle $\langle 100 \rangle$ crystal axes, and the constant c_3 depends on the interband deformation potentials. Stress applied along the [110] or $[1\bar{1}0]$ axis of GaAs gives in-plane shear $\epsilon_{xy} = \epsilon_{yx} \neq 0$. Thus for electrons moving in

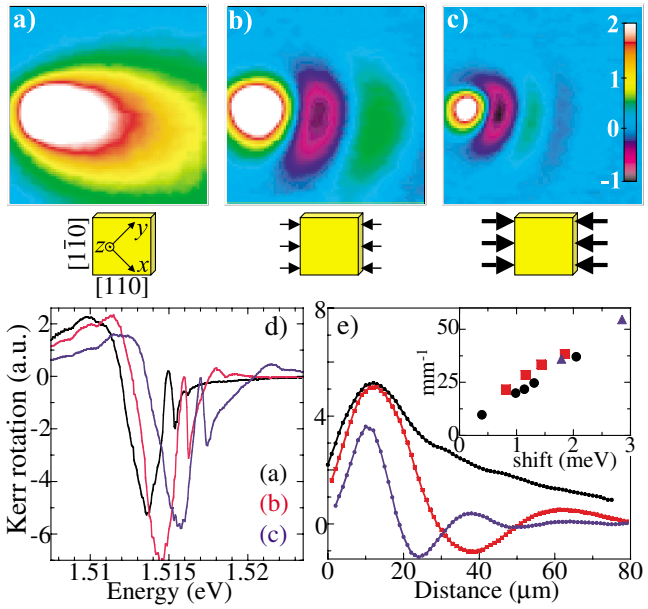

FIG. 2 (color). (a)–(c) 80×80 μm images of 2D spin flow ($E = 10$ V/cm) at 4 K, showing induced spin precession with increasing [110] uniaxial stress. (d) KR vs probe photon energy for the images, showing blueshift of GaAs band edge with stress. (e) Line cuts through the images. Inset: Spatial frequency of spin precession vs band edge shift.

the x-y plane, H_S has similar symmetry to H_R, as it describes an in-plane effective magnetic field, orthogonal to $\mathbf{k}$, with magnitude linear in $|\mathbf{k}|$.

Figs. 2(a)–2(c) show 80×80 μm images of steady-state electron spin flow ($\mathbf{k} \parallel [110]$) in the presence of increasing [110] uniaxial stress. Spin precession is observed, with increasing spatial frequency, indicating a strain-induced effective magnetic field $\mathbf{B}_\epsilon \propto \epsilon_{xy}|\mathbf{k}|$, oriented along $[1\bar{1}0]$. ϵ_{xy} is inferred from the measured blueshifts [see Fig. 2(d)] of $\sim$1 and 2 meV in Figs. 2(b) and 2(c), respectively, indicating strain $|\epsilon_{xy}| \sim 1.5$ and 3.0×10^{-4} (and applied stress $\sim$3.6 and 7.2×10^8 dyn/cm^2) [15]. These strains are small compared to typical $\sim$1% strains due to lattice-mismatched growth; in fact, considerable care was required in sample mounting to avoid spurious and inhomogeneous strains during cooldown. With the cryogenic vise, the stress-induced precession of electron spins is controllable, reversible, and uniform over the sample. Line cuts along [110] [Fig. 2(e)] show many precession cycles ($> 5\pi$ rotation). The inset of Fig. 2(e) confirms that the spatial frequency of the induced precession ($\propto \mathbf{B}_\epsilon$) scales linearly with the band shift ($\propto \epsilon_{xy}$).

Only shear (off diagonal) strain gives $\mathbf{k}$-linear spin-orbit coupling to electron spins. Strain along the $\langle 100 \rangle$ axes, either applied or arising from, e.g., lattice-mismatched [001] growth, should not influence electron spins to lowest order. However, shear strain and $\mathbf{k}$-linear coupling *should* exist in lattice-mismatched samples grown along [110] or [111]. One should not regard $\mathbf{B}_\epsilon$ as arising from electric fields (e.g., stress-induced piezoelectric fields), since such fields are screened in bulk metals.

The line cuts in Fig. 2(e) show that dc spin flows, precessing due to strain, are in phase at large distances from the point of generation. This robust behavior is in marked contrast with the rapid spatial dephasing that occurs when real magnetic fields are used to induce precession in dc spin flows. Figs. 3(a)–3(c) show spin flows with an increasing applied magnetic field ($\mathbf{B}_{\text{app}} \parallel [1\bar{1}0]$), with line cuts in Fig. 3(d). As $\mathbf{B}_{\text{app}}$ increases, the ensemble spin polarization becomes dephased at distances beyond one precession period, particularly when the precession period falls below the spin diffusion length. This pronounced spatial dephasing is due to the randomizing nature of diffusion. The net spin at a remote location is the combined sum of many random walks. Each path takes a different amount of time, giving a different spin rotation, leading to dephasing. Future devices based on magnetic field manipulation of diffusive spin flow may thus be practically limited to a regime requiring π rotation or less. Line cuts through Figs. 2(c) and 3(c) are compared in the inset of Fig. 3(d). Clearly, the spatial coherence of dc spin flows persists over more precession cycles (and greater distance) when the spins are manipulated with strain instead of magnetic field. This is a direct consequence of the $|\mathbf{k}|$-linear nature of $\mathbf{B}_\epsilon$, which correlates precession frequency with electron velocity (and therefore position). Indeed, if electrons moved along only one dimension, the spin flow would not dephase at all (it would still, of course, decohere).

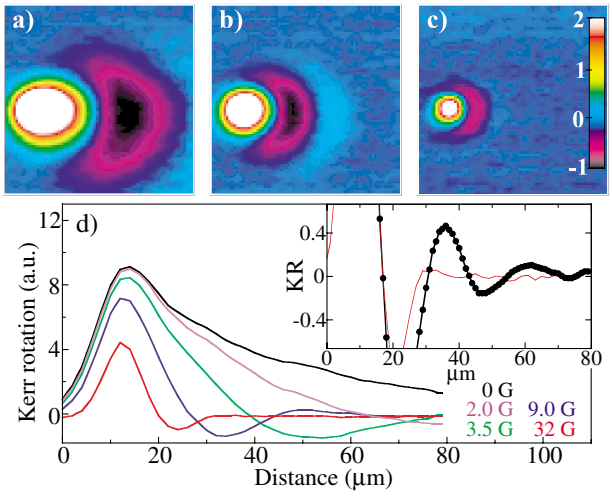

FIG. 3 (color). (a)–(c) 80×80 μm images of 2D spin flow ($E = 10$ V/cm) at 4 K, with increasing applied magnetic field $\mathbf{B}_{\text{app}} = 3.5$, 9, and 32 G along $[1\bar{1}0]$. (d) Line cuts through the images. Inset: Line cuts through Figs. 2(c) (black) and 3(c) (red).

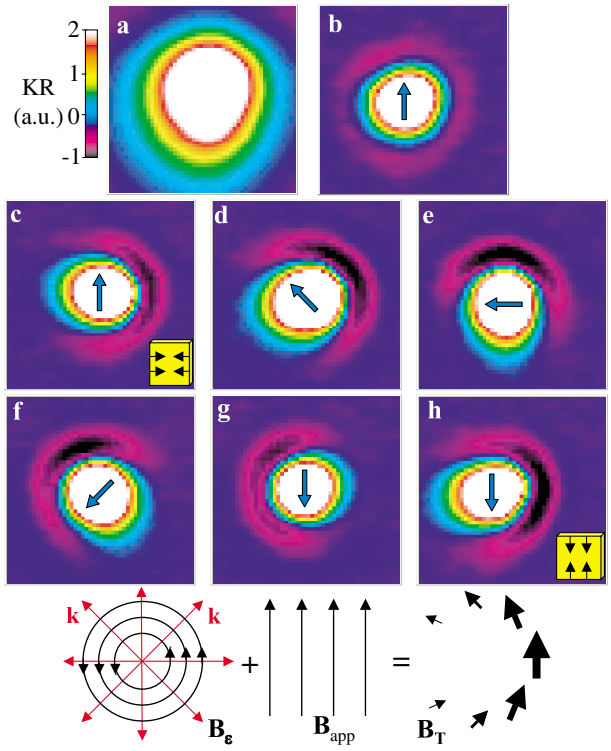

FIG. 4 (color). 50×50 μm images of 2D spin diffusion ($E = 0$) at 4 K. (a) Stress, $\mathbf{B}_{\text{app}} = 0$. (b) Stress = 0, $\mathbf{B}_{\text{app}} = 16$ G along $[1\bar{1}0]$ as shown. (c) $\mathbf{B}_{\text{app}} = 16$ G, with [110] uniaxial stress. Spins diffusing to the right precess; those diffusing to the left do not. Thus $\mathbf{B}_\epsilon$ is chiral for radially diffusing spins (see diagram). (d)–(g) Keeping [110] stress, $\mathbf{B}_{\text{app}}$ is rotated 180° in plane. (h) Stress is switched to $[1\bar{1}0]$, reversing $\mathbf{B}_\epsilon$ chirality.

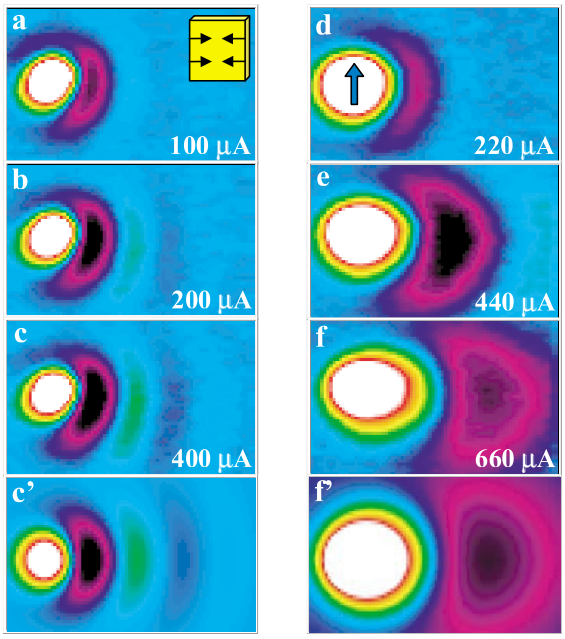

FIG. 5 (color). 50×80 μm images of 2D spin flow at 4 K with increasing $|\mathbf{k}|$ (current). (a–c) With [110] stress and $\mathbf{B}_{\text{app}} = 0$. Spatial period of precession is fixed. (d)–(f) Stress = 0, $\mathbf{B}_{\text{app}} = 6$ G; spatial period varies. Images (c') and (f') are simulations of (c) and (f), using the model described in text.

The images in Fig. 4 confirm that $\mathbf{B}_\epsilon$ is orthogonal to $\mathbf{k}$, such that $\mathbf{B}_\epsilon$ circulates around the point of injection for radially diffusing electrons. Image (a) shows unperturbed spin diffusion (no stress, $\mathbf{B}_{\text{app}} = 0$). In (b), $\mathbf{B}_{\text{app}} = 16$ G along $[1\bar{1}0]$ as shown. Spins precess uniformly, regardless of $\mathbf{k}$, giving a faint annulus of oppositely oriented spins (negative signal) around the injection point. In (c), [110] stress is applied and the image becomes asymmetric. Electrons diffusing to the right ($\mathbf{k} \parallel [110]$) undergo precession, while those diffusing to the left($-\mathbf{k}$) do not. That is, the total field ($\mathbf{B}_T = \mathbf{B}_\epsilon + \mathbf{B}_{\text{app}}$) is finite for spins diffusing to the right, but $\mathbf{B}_T$ is effectively zero for spins diffusing to the left. This image is consistent with a uniform $\mathbf{B}_{\text{app}}$ added to a circulating $\mathbf{B}_\epsilon$, as shown. Maintaining [110] stress, the image asymmetry rotates and ultimately reverses as $\mathbf{B}_{\text{app}}$ is rotated in the x-y plane through 180° (c)–(g). Finally (h), when stress is switched to the $[1\bar{1}0]$ axis, the asymmetry again reverses, indicating the opposite chirality of $\mathbf{B}_\epsilon$.

For comparison with data, we derive and numerically solve the 2D spin drift-diffusion equations. For simplicity, the [110] strain axis is taken here to be the x axis, and the electric and magnetic fields are in the x-y sample plane. The spin polarization is described by the (ρ_x, ρ_y, ρ_z) components of a 2×2 density matrix, where ρ_z gives the ensemble spin density. The equations are $O_1\rho_x = -O_2\rho_z$, $O_1\rho_y = -O_3\rho_z$, and $O_4\rho_z - O_2\rho_x - O_3\rho_y = -G_z$, with operators $O_1 = D\nabla^2 + \mu\mathbf{E}\cdot\nabla - (C_s\varepsilon)^2 D - 1/T_2$, $O_2 = -C_B B_y + C_s\varepsilon(2D\nabla_x + \mu E_x)$, $O_3 = C_B B_x + C_s\varepsilon(2D\nabla_y + \mu E_y)$, and $O_4 = D\nabla^2 + \mu\mathbf{E}\cdot\nabla - 2(C_S\varepsilon)^2 D - 1/T_1$. D is the spin diffusion constant, μ is the mobility, T_2 and T_1 are transverse and longitudinal spin lifetimes, $C_B = \frac{g\mu_B}{\hbar}$, the strain coupling constant C_s is given in Ref. [15], G_z is the spin generation, and ε is the off diagonal strain ϵ_{xy}.

In contrast with the case of an applied magnetic field, both the model and the data reveal a consequence of $\mathbf{k}$-linear $\mathbf{B}_\epsilon$: the spatial period of precession is *independent* of applied electrical bias. Figure 5 confirms this, showing spin flow along [110]. In the presence of strain [Figs. 5(a)–5(c)], the spatial precession period is independent of bias, whereas for the case of applied magnetic field (d)–(f), the spatial precession period clearly increases with increasing bias. Functional "spin transistor" devices based on rotation of spin from, e.g., source to drain contacts [3–6], may well benefit from the freedom to operate at variable electrical bias. Along with spin manipulation via Rashba coupling (also linear in $|\mathbf{k}|$), the spin-orbit coupling of spin flows to shear strains of order 0.01%, as detailed in this work, also affords this flexibility.

This work was supported by the DARPA SpinS and the Los Alamos LDRD programs. We thank S. Kos, P. Littlewood, and I. Martin for valuable discussions.

[1] S. A. Wolf *et al.*, Science **294**, 1488 (2001).
[2] I. Žutić, J. Fabian, and S. Das Sarma, Rev. Mod. Phys. **76**, 323 (2004).
[3] S. Datta and B. Das, Appl. Phys. Lett. **56**, 665 (1990).
[4] J. Schliemann, J. C. Egues, and D. Loss, Phys. Rev. Lett. **90**, 146801 (2003).
[5] K. C. Hall *et al.*, Appl. Phys. Lett. **83**, 2937 (2003).
[6] X. Cartoixà, D. Z.-Y. Ting, and Y.-C. Chang, Appl. Phys. Lett. **83**, 1462 (2003).
[7] J. M. Kikkawa and D. D. Awschalom, Nature (London) **397**, 139 (1999).
[8] Y. Kato *et al.*, Nature (London) **427**, 50 (2004); Phys. Rev. Lett. **93**, 176601 (2004).
[9] M. E. Flatté, J. M. Byers, and W. H. Lau, in *Semiconductor Spintronics and Quantum Computation*, edited by D. D. Awschalom, D. Loss, and N. Samarth (Springer, New York, 2002).
[10] R. Winkler, *Spin-Orbit Coupling Effects in 2D Electron and Hole Systems* (Springer, Berlin, 2003).
[11] Y. A. Bychkov and E. I. Rashba, J. Phys. C **17**, 6039 (1984).
[12] G. E. Pikus and A. N. Titkov, in *Optical Orientation*, edited by F. Meier and B. P. Zakharchenya (North-Holland, Amsterdam, 1984).
[13] D. G. Seiler, B. D. Bajaj, and A. E. Stephens, Phys. Rev. B **16**, 2822 (1977).
[14] M. Cardona, V. A. Maruschak, and A. N. Titkov, Solid State Commun. **50**, 701 (1984); M. Cardona, N. E. Christensen, and G. Fasol, Phys. Rev. B **38**, 1806 (1988).
[15] G. L. Bir and G. E. Pikus, *Symmetry and Strain-Induced Effects in Semiconductors* (Halstead, New York, 1974).